

Spheromak formation and sustainment by tangential boundary flows

Pablo Luis García-Martínez and Ricardo Farengo
Instituto Balseiro and Centro Atómico Bariloche

(Dated: July 21, 2021)

The nonlinear, resistive, 3D magnetohydrodynamic equations are solved numerically to demonstrate the possibility of forming and sustaining a spheromak by forcing tangential flows at the plasma boundary. The method can be explained in terms of helicity injection and differs from other helicity injection methods employed in the past. Several features which were also observed in previous dc helicity injection experiments are identified and discussed.

Spheromak plasmas have been formed using several different techniques [1, 2]. The existence of multiple formation methods clearly shows that the spheromak is a preferred (lowest energy) state toward which a magnetohydrodynamic (MHD) system naturally evolves when the appropriate boundary conditions are imposed. The physical process responsible for the formation is magnetic relaxation: on the time scale of MHD instabilities the plasma relaxes to the minimum energy state compatible with its magnetic helicity content (which remains approximately constant) [3]. Once formed, the spheromak will decay in a resistive time scale because resistivity does dissipate magnetic helicity. For this reason, the sustainment of the configuration during times longer than the resistive decay time requires some helicity injection method. Since relaxation operates on a shorter time scale, the spheromak configuration is maintained regardless of the details of the specific helicity injection mechanism. Some particular examples are the coaxial helicity injection method (CHI) [4–6], the merging of helicity-carrying filaments (MHF) [7] and the helicity injected torus with steady inductive helicity injection (HIT-SI) [8].

In this Letter we report the first evidence coming from nonlinear, resistive, 3D MHD numerical simulations that demonstrate the possibility of forming and sustaining a spheromak by forcing tangential flows at the plasma boundary. The method can be explained in terms of helicity injection and differs from other helicity injection methods employed in the past (CHI, MHF and HIT-SI).

An enhanced helicity injection mode was recently reported in spheromak experiments with large plasma rotation [9]. Although not analyzed in terms of boundary flows, this observation could support the feasibility of the mechanism proposed and studied in this Letter.

We model the plasma using the resistive MHD equations with finite viscosity and zero β . The evolution equations for \mathbf{u} and \mathbf{B} are:

$$\partial_t \mathbf{u} + \mathbf{u} \cdot \nabla \mathbf{u} = (\mathbf{J} \times \mathbf{B})/\rho_0 + \nu \nabla^2 \mathbf{u}, \quad (1)$$

$$\partial_t \mathbf{B} + \nabla \times \mathbf{E} = 0, \quad (2)$$

where $\mathbf{E} = -\mathbf{u} \times \mathbf{B} + \eta \mathbf{J}$ and $\Pi = (\nabla \mathbf{u} + \nabla \mathbf{u}^T) - (2/3) \times (\nabla \cdot \mathbf{u})$ (see Ref. [10] for further details). These equations are normalized with a (chamber radius), ψ_G (imposed

flux) and c_A (Alfvén speed). In addition, \mathbf{B} and \mathbf{J} are scaled with $\sqrt{\mu_0}$. Time is expressed in units of the Alfvén time $\tau_A = a/c_A$. The normalized resistivity η and the kinematic viscosity ν are set to 5×10^{-5} . With these values the resistive time is $\tau_r \sim 800$ (defined as in Ref. [11]). The resulting system is solved with the Versatile Advection Code [12].

The domain is a cylinder of elongation $h/a = 1$, with perfectly conducting wall conditions ($\mathbf{B} \cdot \mathbf{n} = 0$ and $\mathbf{J} \times \mathbf{n} = 0$) and vanishing velocity ($\mathbf{u} = 0$) at the cylindrical boundary ($r = a$) and the top end ($z = h$). At the bottom end we impose the poloidal flux: $\psi(r, z = 0) = C\psi_G(r/a)^2(1 - r/a)^3$, where $C = 28.935$ is a constant and ψ_G is the maximum flux imposed by the gun. This geometry has been used to model the Spheromak Experiment (SPHEX) [13]. If $\mathbf{u} = 0$ is imposed at $z = 0$ the full set of boundary conditions leads to vanishing helicity and energy fluxes across the boundary. Recently, these conditions have been applied to study the decay of configurations representative of electrostatically driven spheromaks with open field lines [14].

Imposing tangential flows at a boundary intercepted by magnetic flux may result in the injection of helicity, as can be inferred from the equation $dH/dt = -2 \int_V \eta \mathbf{J} \cdot \mathbf{B} dV - 2 \oint_{\partial V} [(\mathbf{A} \cdot \mathbf{B})(\mathbf{u} \cdot \mathbf{n}) - (\mathbf{A} \cdot \mathbf{u})(\mathbf{B} \cdot \mathbf{n})] dS$ (neglecting electrostatic fields). The last term on the right gives the helicity injection produced by motions of the footpoints of the penetrating (open) magnetic field [15]. Boundary shearing of magnetic fields has been applied in the past to study reconnection events in low- β plasmas relevant to the solar corona [16].

The computations presented in this Letter have $u_r = u_z = 0$ and $u_\theta = u_0 \max[0, 25(2/5 - r)r]$, at $z = 0$. This flow produces helicity injection across the bottom end of the cylinder because $A_\theta = \psi(r, z = 0)/(2\pi r)$ there. The initial condition is the vacuum magnetic field and zero velocity inside the chamber. Setting $u_0 = -0.1$ we obtained the results shown in Figs. 1, 2 and 3. The results of two more runs, with u_0 equal to -0.05 and -0.2 , are discussed in the context of Figs. 4 and 5.

The evolutions of the maximum poloidal flux (ψ_{ma}) and the toroidal flux across the entire poloidal plane (Φ) are shown in Fig. 1 (a). For $t < 45$, ψ_{ma} remains at the constant imposed value, while there is a build up

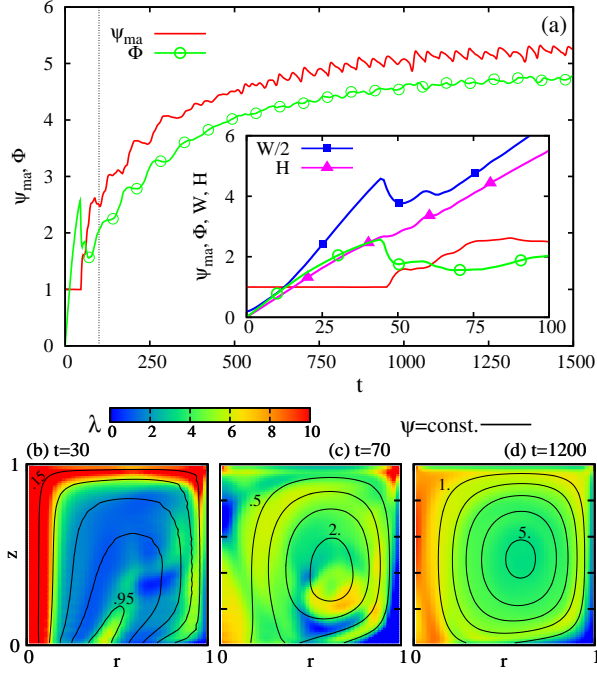


FIG. 1: (Color online) Evolution of ψ_{ma} and Φ (a). In the inset, the evolution for $t < 100$ is showed in more detail. In addition the (halved) magnetic energy and the helicity are shown. Colormaps of λ and ψ contours in the poloidal plane are shown at three different times (b)-(d).

of Φ . Magnetic energy and helicity (computed using a gauge invariant definition [17]) are shown in the inset of Fig. 1 (a). At $t \sim 45$, a relaxation event which produces significant energy dissipation at approximately constant helicity and flux conversion from toroidal to poloidal is clearly observed. The kinetic energy K (not shown) is small during the whole evolution (K/W has a peak of 0.1 at $t \sim 50$ and remains below 0.01 during sustainment). Panels (b), (c) and (d) of Fig. 1 show contours of ψ and colormaps of λ (where $\lambda = \mathbf{J} \cdot \mathbf{B}/B^2$, is computed using the $n = 0$ component of the toroidal Fourier decomposition of \mathbf{B}) at different times. At $t = 30$, λ is strongly peaked near the geometric axis and no closed ψ contours are identified. After the relaxation event ($t = 70$) λ is redistributed and closed ψ contours appear, indicating the formation of a spheromak configuration. The poloidal and toroidal fluxes continue to increase until $t \sim 700$ and afterwards a quasi stationary state is sustained for one resistive time, indicating that a balance between helicity injection and dissipation has been reached. The ψ and λ distributions shown in Fig. 1 (d) are representative of this quasi-steady state.

It is well known that spheromak formation and sustainment necessarily involves non-axisymmetric activity. The magnetic field lines (followed from fixed positions at the bottom end) plotted in Fig. 2 clearly show that

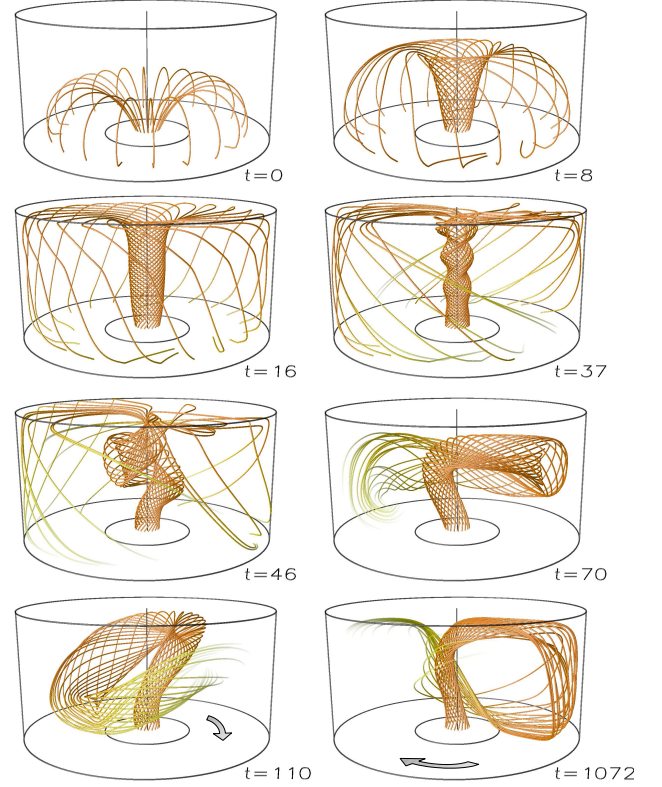


FIG. 2: (Color online) Twenty field lines followed from fixed positions at the bottom end, for eight different times. The opacity of the lines is gradually decreased when their length L is longer than 4, and they become completely transparent when $L \geq 5$. The structure observed at $t = 110$ is almost in its final saturated state (observed at $t = 1072$) and rotates clockwise (when viewed from top).

our computations reproduce this feature. The initial field lines of the vacuum solution ($t = 0$) expand and twist ($t = 8$) forming a central current-carrying column ($t = 16$). As the current through the central column increases and the field lines increase their twisting, the configuration eventually becomes unstable ($t = 37$) and the typical helical structure of a kink instability quickly develops ($t = 46$). This instability, with dominant toroidal wavenumber $n = 1$, saturates at a relatively small and fixed amplitude ($W_{n=1}/W_{n=0} \sim 0.01$ during sustainment, see Fig. 4) causing the central column to adopt an almost fixed helical shape which rotates as indicated in Fig. 2 ($t = 110$ and $t = 1072$). Our results reproduce the experimental observation of a fixed rotating helical structure with a strongly asymmetric return column [18]. In contrast with our case (driven purely by boundary flows), the plasma in those experiments was driven electrostatically. We note, however, that the presence of an inductive component in the electric field when magnetic fluctuations were active, was also reported [18].

It is important to note that the motion of this struc-

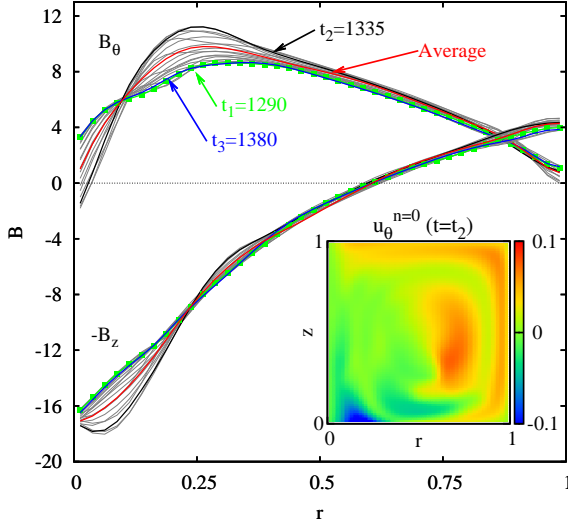


FIG. 3: (Color online) Twenty instantaneous profiles (between t_1 and t_3) of B_θ and B_z , at $z = h/2$ and $\theta = 0$. The profile of the time averaged fields is also shown. The $n = 0$ component of the toroidal velocity at t_2 is shown in the inset.

ture is produced by the coherent oscillation of the $n = 1$ mode and not by a rigid rotation of the plasma. This is shown in Fig. 3 where the radial profiles of B_θ and B_z , at $z = h/2$ and $\theta = 0$, are plotted for several times between $t_1 = 1290$ and $t_3 = 1380$. The profiles at t_1 and t_3 are almost identical, indicating that the structure makes one turn every 90 Alfvén times. Such rotation is much slower than that expected from the imposed $u_0 = -0.1$ at $r = 0.2$. Furthermore, the plasma toroidal velocity reverses its sign as can be observed in the inset of Fig. 3 (this velocity colomap is plotted at $t_2 = 1335$ but it is representative of the flow pattern during sustainment, $700 < t < 1500$). This velocity reversal is also observed in the other two runs presented in this work and it is evidently a feature of the saturated state of the instability. However, the specific reason for this velocity reversal is still not yet understood.

The evolution of ψ_{ma} and the poloidal magnetic field near the wall (total $B_z|_w$ and $B_z^{n=0}|_w$) at $z = h/2$ and $\theta = 0$ are shown for three values of u_0 in Fig. 4 (a)-(c). The magnetic energy (relative to the initial energy) of the modes $n = 0$, $n = 1$ and $n = 2$ is shown in Fig. 4 (d). These results indicate that increasing the helicity injection rate (which is linear in u_0) leads to configurations with higher flux amplification and more energy in the $n = 0$ mode. Nevertheless, the energy associated to the $n > 0$ modes (in particular the $n = 1$) saturates at a fixed amplitude, which is roughly independent of u_0 . This implies a lower level of fluctuations relative to the $n = 0$ mode at higher helicity injection rates. A similar saturation mechanism has also been observed in experiments [18, 19].

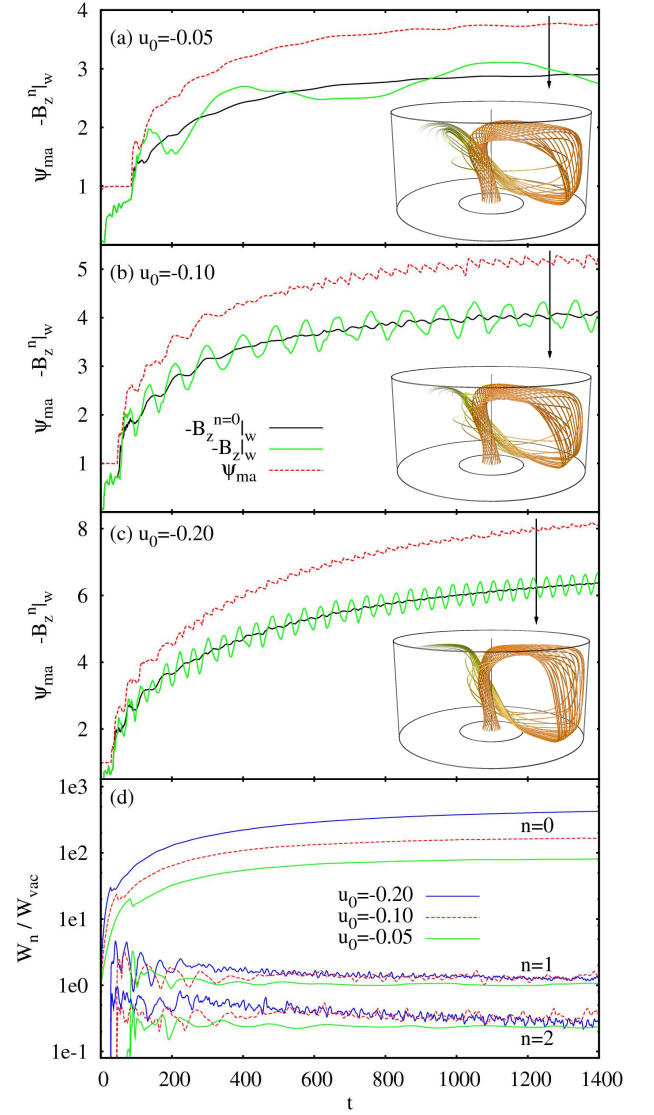


FIG. 4: (Color online) Evolution of ψ_{ma} and the poloidal magnetic field near the wall (total $B_z|_w$ and $B_z^{n=0}|_w$) for three values of u_0 (a)-(c). Field lines showing the central open flux column are presented in each case at the time indicated by the arrow. Magnetic energy of the modes $n = 0, 1$ and 2 (d).

The oscillation of the fluctuation in the poloidal magnetic field near the wall ($B_z|_w$) is clearly observed in Figs. 4 (a)-(c). As discussed previously, this corresponds to a coherent oscillation which produces the rotation of the magnetic structures shown in the insets of Figs. 4 (a)-(c). Note that the rotation frequency increases rapidly with the helicity injection rate. Another important observation is that the rotation frequency is not the same, in general, that the frequency of the oscillating dynamo term that amplifies ψ_{ma} (which depends on the correlation of the fluctuations of \mathbf{u} and \mathbf{B}). This is specially clear in Fig. 4 (b).

The MHD activity maintains the configurations ob-

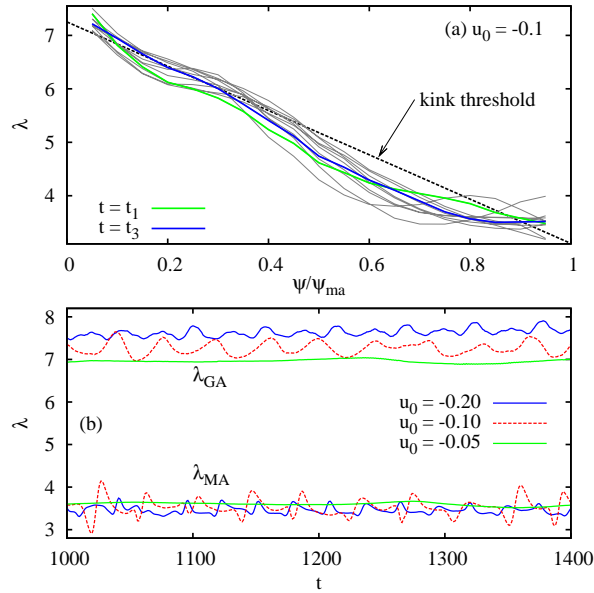


FIG. 5: (Color online) $\lambda(\psi)$ profiles for the case with $u_0 = -0.1$ at ten times between t_1 and t_3 (a). The kink instability threshold is indicated. Time evolution of λ at the geometric axis (λ_{GA}) and at the magnetic axis (λ_{MA}), for the three runs (b).

tained for the three different values of u_0 close to the kink stability boundary. This is shown in Fig. 5. The $\lambda(\psi)$ profiles of the $n = 0$ mode are plotted in Fig. 5 (a), for the case with $u_0 = -0.1$, at ten times between t_1 and t_3 (ψ is normalized with ψ_{ma}). The indicated kink instability threshold is a linear $\lambda(\psi)$ profile, which has a slope $\alpha = -0.4$ [20]. Fig. 5 (b) shows the evolution of the λ values at the geometric axis (λ_{GA}) and at the magnetic axis (λ_{MA}) for the three runs. The behavior observed here is similar to that described in previous experiments [19, 20]. The configuration evolves around the kink stability boundary as a result of the competition between the external forcing, which tends to steepen the λ profile, and the relaxation, which tends to flatten it.

In summary, we demonstrated the possibility of forming and sustaining a spheromak by imposing tangential flows at the boundary. Several aspects of the process were described. The relationship between our results and the existing experimental evidence was discussed. The fact that our simulations reproduce many features observed in electrostatic CHI experiments is interpreted as follows. Since the spheromak is formed and sustained by the relaxation of an unstable configuration, the dynamics of the process should be independent of the details on how this configuration is driven unstable. In this sense, this Letter not only provides evidence on a new spheromak formation and sustainment mechanism, but it also pro-

vides valuable information pertaining to the dynamics of the kink instability in electrostatically driven spheromaks. To conclude, we note that although our results were obtained for a spheromak, boundary plasma flows could also be used to inject helicity in other configurations (i.e. spherical tokamaks).

Financial support from the UNCuyo and the ANPCyT is acknowledged. P.L.G.-M. is supported by CONICET.

-
- [1] T. R. Jarboe, *Plasma Physics and Controlled Fusion* **36**, 945 (1994).
 - [2] T. R. Jarboe, *Physics of Plasmas* **12**, 058103 (2005).
 - [3] J. B. Taylor, *Reviews of Modern Physics* **58**, 741 (1986).
 - [4] P. K. Browning, G. Cunningham, S. J. Gee, K. J. Gibson, A. Al-Karkhy, D. A. Kitson, R. Martin, and M. G. Rusbridge, *Physical Review Letters* **68**, 1718 (1992).
 - [5] E. B. Hooper, L. D. Pearlstein, and R. H. Bulmer, *Nuclear Fusion* **39**, 863 (1999).
 - [6] T. R. Jarboe, I. Henins, A. R. Sherwood, C. W. Barnes, and H. W. Hoida, *Physical Review Letters* **51**, 39 (1983).
 - [7] S. Woodruff, D. N. Hill, B. W. Stallard, R. Bulmer, B. Cohen, C. T. Holcomb, E. B. Hooper, H. S. McLean, J. Moller, and R. D. Wood, *Phys. Rev. Lett.* **90**, 095001 (2003).
 - [8] T. R. Jarboe, W. T. Hamp, G. J. Marklin, B. A. Nelson, R. G. O'Neill, A. J. Redd, P. E. Sieck, R. J. Smith, and J. S. Wrobel, *Physical Review Letters* **97**, 115003 (2006).
 - [9] Z. Wang, J. Si, and H. Li, *Journal of Fusion Energy* **26**, 233 (2007).
 - [10] P. L. García Martínez and R. Farengo, *Physics of Plasmas* **16**, 082507 (2009).
 - [11] V. A. Izzo and T. R. Jarboe, *Physics of Plasmas* **10**, 2903 (2003).
 - [12] G. Tóth, *Astrophysical Letters & Communications* **34**, 245 (1996), URL www.phys.uu.nl/~toth/.
 - [13] D. P. Brennan, P. K. Browning, and R. A. M. van der Linden, *Physics of Plasmas* **9**, 3526 (2002).
 - [14] P. L. García Martínez and R. Farengo, *Physics of Plasmas* **16**, 112508 (2009).
 - [15] M. A. Berger, in *Measurement Techniques in Space Plasmas Fields*, edited by M. R. Brown, R. C. Canfield, & A. A. Pevtsov (1999), pp. 1+.
 - [16] K. Galsgaard and Å. Nordlund, *Journal of Geophysical Research* **101**, 13445 (1996).
 - [17] J. M. Finn and T. M. Antonsen, *Comments Plasma Physics and Controlled Fusion* **33**, 1139 (1985).
 - [18] R. C. Duck, P. K. Browning, G. Cunningham, S. J. Gee, A. al-Karkhy, R. Martin, and M. G. Rusbridge, *Plasma Physics and Controlled Fusion* **39**, 715 (1997).
 - [19] D. M. Willett, P. K. Browning, S. Woodruff, and K. J. Gibson, *Plasma Physics and Controlled Fusion* **41**, 595 (1999).
 - [20] S. O. Knox, C. W. Barnes, G. J. Marklin, T. R. Jarboe, I. Henins, H. W. Hoida, and B. L. Wright, *Physical Review Letters* **56**, 842 (1986).